

Impact of Morphology on Printed Contact Performance in Carbon Nanotube Thin-Film Transistors

Jorge A. Cardenas, Sophia Upshaw, Nicholas X. Williams, Matthew J. Catenacci, Benjamin J. Wiley, and Aaron D. Franklin*

Silver nanoparticles (NPs) are the most widely used conductive material throughout the printed electronics space due to their high conductivity and low cost. However, when interfacing with other prominent printed materials, such as semiconducting carbon nanotubes (CNTs) in thin-film transistors (TFTs), silver is suboptimal when compared to more expensive or less conductive materials. Consequently, there would be significant value to improving the interface of printed silver to CNT films. In this work, the impact of nanostructure morphology on the electrical properties of printed silver and nanotube junctions in CNT-TFTs is investigated. Three distinct silver morphologies (NPs, nanoflakes – NFs, and nanowires – NWs) are explored with top- and bottom-contact configurations for each. The NF morphology in a top-contact configuration is found to yield the best electrical interface to CNTs, resulting in an average contact resistance of $1.2 \text{ M}\Omega \cdot \mu\text{m}$. Beyond electrical performance, several trade-offs in morphology selection are revealed, including print resolution and process temperature. While NF inks produce the best interfaces, NP inks produce the smallest features, and NW inks are compatible with low processing temperatures ($<80^\circ\text{C}$). These results outline the trade-offs between silver contact morphologies in CNT-TFTs and show that contact morphology selection can be tailored for specific applications.

1. Introduction

Emerging applications, such as those in the Internet of Things (IoT) revolution, have motivated the advancement of low-cost printing methods for manufacturing the next generation of electronics.^[1–4] There are now numerous printing approaches that span from high throughput methods, such as screen and gravure printing, to highly customizable, direct-write methods, such as

inkjet and aerosol jet printing. Common among each of these printing methods are solution-based functional electronic inks, which are composed of electronically functional particulates, binders (adhesion or solubility modifiers), additives (rheology modifiers), and solvents.^[5] Together, functional inks along with the various printing approaches could enable the development of emerging applications such as ubiquitous, flexible, and even biointegrated electronics, which have previously been inaccessible to the traditional semiconductor-based manufacturing technologies.^[6] Throughout the printed electronics space, the most commonly used ink particulates are silver (Ag) nanoparticles (NPs), which are advantageous due to their superb dispersion stability, oxidation resistance, high conductivity, and relatively low cost.^[7] Compared with other inorganic inks, such as gold and platinum NPs, silver NP inks are much cheaper and can be sintered at lower temperature.^[8] Further, compared with conductive organic inks, silver is significantly more conductive and has better performance stability in ambient conditions.^[9,10]


Thus, silver strikes the best balance between cost, stability, and performance amongst conductive and printable materials.

Among the most prominent active devices that commonly utilize printed silver NP electrodes is the carbon nanotube thin-film transistor (CNT-TFT), which has shown promise as a fully printable device for display, sensing, and circuit applications.^[11–15] The network films of semiconducting carbon nanotubes (s-CNTs), which are the channels in CNT-TFTs, are inherently flexible and lend themselves to low-temperature, solution-based processing.^[16–19] These favorable attributes have enabled demonstrations of printed, low-temperature processed, stretchable, and wearable CNT-TFTs.^[20–25] CNT-TFTs stand out in the printed and flexible electronics space due to their balance between performance, printability, and flexibility. Compared to organic TFTs, CNT-TFTs exhibit much higher mobilities, and are much more stable and resilient to environmental conditions. With respect to metal oxide TFTs, CNT-TFTs are more flexible, stretchable, and have much lower process temperature requirements resulting in lower fabrication costs.^[26]

One of the main challenges for printed CNT-TFTs are the contact electrodes, which can be a source for increased

J. A. Cardenas, S. Upshaw, N. X. Williams, Prof. A. D. Franklin
Department of Electrical and Computer Engineering
Duke University
Durham, NC 27708, USA
E-mail: aaron.franklin@duke.edu

Dr. M. J. Catenacci, Prof. B. J. Wiley, Prof. A. D. Franklin
Department of Chemistry
Duke University
Durham, NC 27708, USA

 The ORCID identification number(s) for the author(s) of this article can be found under <https://doi.org/10.1002/adfm.201805727>.

DOI: 10.1002/adfm.201805727

variability and hampered device performance.^[27–29] There have been limited studies to address printed contact issues in CNT-TFTs. One of these works includes a comparison between silver, gold, and metallic CNT (m-CNT) contacts, which demonstrated that m-CNT and gold contacts produced the best performing devices compared to traditional silver NP contacts,^[27] despite silver's advantageous conductivity properties. However, more work still needs to be done beyond the previously mentioned study to improve printed contacts, specifically with respect to decreasing costs and improving conductivity while simultaneously minimizing contact resistance. In an attempt to improve the electrical properties of silver films, which still have the potential to fulfill the previously mentioned requirements, another study by Stewart et al.^[30] has demonstrated that high aspect ratio silver nanostructures (long silver nanowires [NWs]) yield both lower resistivity films and the ability to process those films at substantially lower sintering temperatures. However, with respect to printed electronics, this study did not address the challenges associated with printing inks consisting of high aspect ratio nanostructures, nor did it comment on the interfacial interaction of those nanostructures with other materials, such as CNTs. In order to fully evaluate the promise of using silver films consisting of larger nanostructures, the interfacial properties of these films must be evaluated in the context of printed devices.

In this work, we discovered that appropriate selection of nanostructure morphology for printed silver contacts in CNT-TFTs can yield improved contact interfaces, resulting in better on-state performance. Additionally, we found that certain contact configurations can significantly reduce device-to-device variability. Hundreds of devices were fabricated using an aerosol jet printer to systematically investigate the role of contact morphology in CNT-TFT performance. Three silver morphologies were studied (NPs, NWs, and nanoflakes – NFs, as depicted in Figure 1) using two separate contact configurations (top- and bottom-contact, shown in Figure 2a,b, respectively), all of which were evaluated using the transfer length method (TLM) with CNT-TFTs. In top-contacted devices, the NF morphology yields the best electrical interface to CNTs, boosting the resulting on-state performance by up to 75%. The contact resistance from the printed CNT-TFTs with Ag NF contacts is among the lowest reported to date, even among other materials such as gold and m-CNTs. Ultimately, there are key trade-offs in contact morphology selection, with NF contacts producing optimal electrical performance, NP contacts offering the highest printing resolution, and NW contacts enabling low-temperature (<80 °C) processing. These findings outline the trade-offs between contact morphology, device fabrication, and performance in CNT-TFTs, providing important guidance in designing printed CNT-TFT devices.

2. Results and Discussion

All devices were fabricated using an Optomec AJ300 Aerosol Jet printer—a direct-write printer in which ink is aerosolized either ultrasonically or pneumatically and is jetted through a nozzle using an inert nitrogen carrier gas flow. The printer nozzle focuses the ink/gas stream toward the substrate using a secondary inert sheath gas flow. This process also prevents ink from coming into contact with the nozzle sidewalls, which inhibits nozzle clogging. A schematic representation of this process is given in Figure 1a, which also depicts the general structure of all CNT-TFTs printed in this work. The channel of each CNT-TFT consists of a randomly oriented s-CNT network, a scanning electron microscope (SEM) image of which can be seen in Figure 1b, printed from a commercially available ink (IsoSol-S100 from Nanointegris Inc.). The Ag NPs (Figure 1c) is the most common of the three morphologies studied and is printed from a commercially available ink (Ag40× from UTdots Inc.). Ag NFs (Figure 1d) is the least common morphology used to contact CNT-TFTs and is also printed from a commercially available ink (HPS-108AE1 from Novacentrix Inc.). The last morphology, Ag NWs (Figure 1e), is a common silver morphology in many research areas for conductive transparent films and coating applications. To the best of our knowledge, there are no current commercial options for an aerosol jet-printed Ag NW ink; therefore, we have developed our own ink based on previous work.^[20]

Substrate-gated CNT-TFTs were used in this study to allow for uniformity in gate structure with electrostatic control of the channel and consideration of top- and bottom-contact

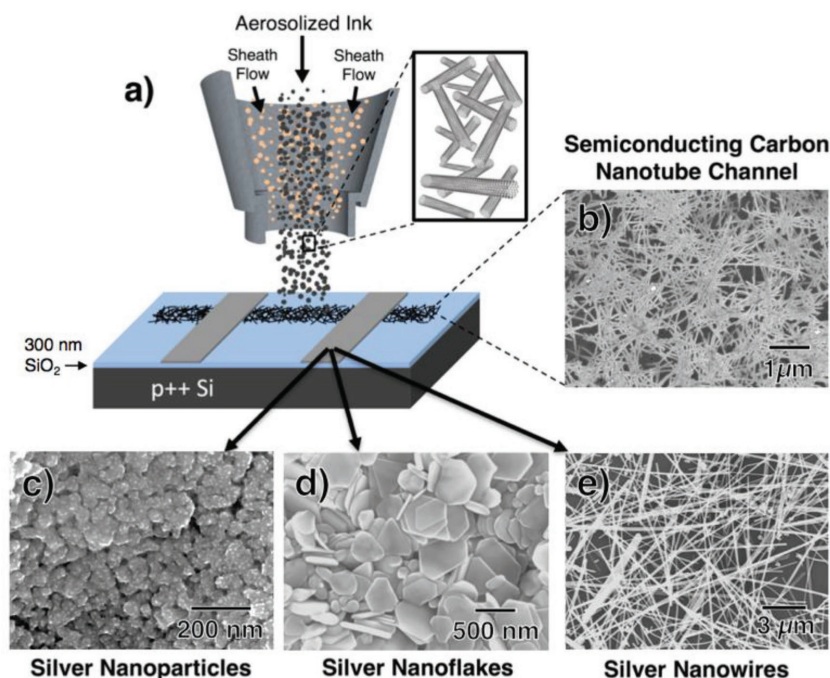


Figure 1. Schematic comparison of three Ag contact morphologies explored in CNT-TFTs. a) Illustration of the aerosol jet deposition process and the printed CNT-TFT device structure. b) SEM image of the randomly oriented CNT network serving as the TFT channel. c–e) SEM images of the silver contact morphologies compared in this study.

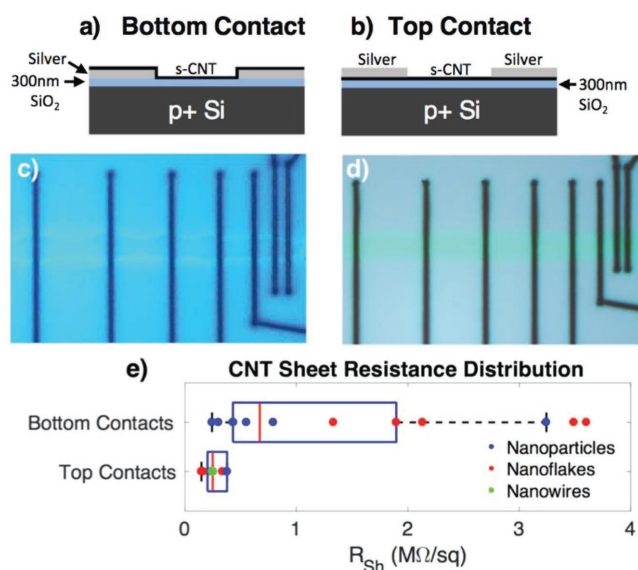


Figure 2. Comparison between bottom- and top-contacted CNT-TFTs. Schematic illustrations of a) bottom-contacted devices and b) top-contacted devices. Representative optical images of TLM arrays consisting of c) bottom-contacted CNT-TFTs showing nonuniform CNT films and d) top-contacted CNT-TFTs showing uniform CNT films. e) CNT R_{sh} distribution between bottom- and top-contacted devices, with top-contacted devices showing superior film characteristics across multiple sets of TLM structures, independent of contact material.

geometries. Substrates were p-doped Si with 300 nm SiO_2 top layers used for the gate dielectric. The process flow for fabricating both top- and bottom-contacted devices is illustrated in Figure S1 in the Supporting Information. For the top-contacted devices, the CNTs were printed prior to the contacts, whereas for bottom-contacted devices, they were printed after the contacts. Prior to CNT printing, the substrates were immersed in poly-L-lysine (PLL) to functionalize the SiO_2 surface and promote CNT adhesion. After CNT printing, the substrates were rinsed with toluene to remove residual organics from the film. Silver contacts were printed using either the Ag NP, NF, or NW ink and then baked.

Contact configuration results are presented in Figure 2, which shows that the uniformity of top-contacted devices was greater than that of bottom-contacted devices across multiple TLM structures. The difference in CNT film uniformity between top- and bottom-contacted devices can be attributed to the presence of the contacts during the CNT rinse step (representative top-down optical images of TLM structures are given in Figure 2c,d). For top-contacted devices, CNTs are printed on a pristine SiO_2 surface, where no other physical features are present to impede the flow of the rinse. For bottom-contacted devices, the presence of silver films on the surface of the substrate impedes the uniform flow of the toluene rinse, resulting in nonuniform channel characteristics, particularly near the contacts. In conjunction with the physical variances, upon extracting the sheet resistance of the CNT films (see Figure 2e), it was found that the bottom-contact sheet resistance distribution was far broader than that of the top-contacts. Additionally, the NF contacts (which have the largest trace heights) produced the largest s-CNT sheet resistance values with the broadest spread, which indicates that larger contact heights exacerbate this deleterious rinsing effect.

Prior to directly comparing the effect of contact morphology on device performance, the physical and electrical characteristics of the individual traces will first be discussed. As was found in previous reports by Stewart et al.,^[30] nanostructure aspect ratio is inversely related to the maximum process temperature required to produce sufficiently conductive films. For this reason, the sintering temperatures required for NP and NF films were 180 and 150 °C, respectively, while the high aspect ratio NWs produced conductive films without any required sintering. While printing the NWs, the printer platen was held at 80 °C to assist with ink evaporation and uniformity of the films. Printing at temperatures lower than 80 °C resulted in excess solvent accumulation on the substrate and poor film uniformity. In contrast, the uniformity of NP and NF films were much less sensitive to changes in platen temperature, but were printed at platen temperatures of 60 °C to minimize linewidth and keep process conditions relatively constant between inks. In addition to the 60 °C platen temperature, the NP and NF films would both undergo a much higher temperature sinter following the printing.

In addition to the sintering requirements, we also find that film surface roughness corresponds directly to particle length and surface area (Figure 3a,b). The trace profile, as presented in Figure 3c (full trace profiles are provided in Figure S2 in the Supporting Information), shows that the NF ink produced the thickest and widest traces. As expected from the analysis of particle dimension, the NPs had the smallest trace profile between the three inks; however, throughout this study, the NP overspray was highly variable between prints. As indicated in both the surface roughness and profile measurements (as well as SEM images in Figure S3 in the Supporting Information), the NW films are the most porous and least dense among the three morphologies. The NF and NP films both exhibited low sheet resistance values due to their large trace thicknesses and high film densities. The NW films had relatively high sheet resistance that is partially attributed to the low NW density in the film compared to the other two inks. The resulting sheet resistance values (Figure 3d) were obtained using the 4-point probe method. As was found by Stewart et al.,^[30] sintering the NW films up to 200 °C did not produce significant improvements in sheet resistance measurements.

As discussed previously, device results were evaluated using TLM structures across multiple chips. The TLM structures consist of an array of adjacently placed CNT-TFTs with channel lengths ranging from 50 to 800 μm . For a given channel length, throughout the entire set of chips, NF-contacted devices exhibited superior on-state performance when compared to NP- and NW-contacted devices. A representative set of transfer and subthreshold characteristics for CNT-TFTs of the three different contact morphologies with $L_{ch} = 200 \mu\text{m}$ are plotted in Figure 4a. These results were reproduced with minimal variability when printing multiple devices with the same channel length across each contact morphology on the same chip (results of which are presented in Figure S4 in the Supporting Information). Relevant on-state performance metrics, such as width-normalized transconductance and mobility, were then extracted and compared across the three contact morphologies (see Figure 4b,c, respectively). As has been previously found throughout relevant CNT-TFT literature, we find that

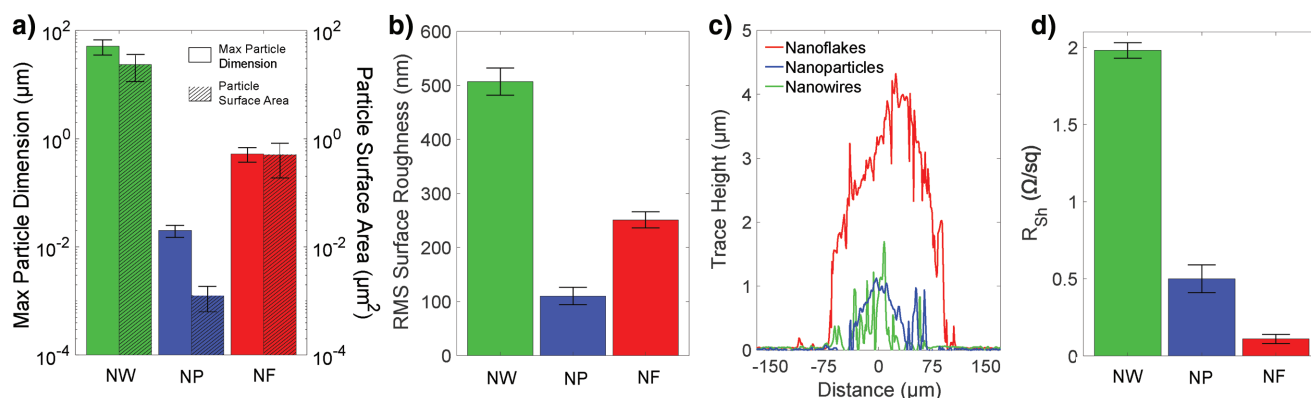


Figure 3. Comparison of film characteristics between silver contact morphologies. a) Morphological properties of the three nanoink particulates, indicating particle diameter (solid, left axis) and particle surface area (hatched, right axis). b) Printed line surface roughness, which closely matches the morphological properties of each ink. c) Representative trace profiles, with NFs having the largest profile, NPs having the smallest profile, and NWs having the roughest and most porous profile. d) Sheet resistance comparison of 2×6 mm rectangular films.

improvements in mobility, transconductance, and on-current were correlated with lower contact resistance.^[27–29]

There may be multiple factors influencing the more favorable NF contacts; among these, silver sheet resistance and contact length are not considered to be relevant. For one, sheet

resistance of the silver is negligible as it is dwarfed by the much higher resistance of the contact interface. Meanwhile, contact length (distance over which the metal contact overlaps the semiconducting CNT thin-film channel) in these devices is several times the transfer length (estimated from TLM data), which was only a few microns for each film morphology; hence, the different printed line widths (which define contact lengths) would not be impacting performance.^[31] It should also be noted that process temperature is not a significant factor, as the NW devices were sintered at temperatures up to 200 °C and resulted in no significant reduction in the measured contact resistance.

Factors that are considered contributory to the superior NF contact performance (Figure 4d) are the aerial surface coverage, particle surface area, and film surface roughness, all of which are factors of contact area. The NF films exhibit a high aerial surface coverage (Figure 1d), moderate particle size (Figure 3a), and intermediate film roughness (Figure 3b). Combined, these attributes produce the most conformal contact to the underlying CNT network. Although NPs also have a high aerial surface coverage, the NP films exhibit intermediate contact resistance due to small particle surface area and low surface roughness. The NW films have the largest particle sizes and roughest surfaces; however, they are not very dense and are highly porous, leading to low surface coverage and low corresponding contact area. It should be emphasized that low contact resistance is not intrinsic to particle morphology and that increasing the NW film density and aerial surface coverage should reduce the NW film contact resistance to the CNT thin film. In addition to modifying contact morphology, contact resistance can also be decreased by increasing the underlying CNT film density, as has been previously demonstrated.^[28,29]

To benchmark the devices fabricated in this study to others from the literature, we have assembled a comparison table of CNT-TFTs with printed contacts in Table 1. As can be seen from the width-normalized contact resistance column, the NF devices produced in this work exhibited the lowest average contact resistance, which lead to relatively high on-state performance metrics such as mobility and transconductance. The NF contact resistance produced in this work is lower than that of gold NP and m-CNT contacts, indicating that deviating away

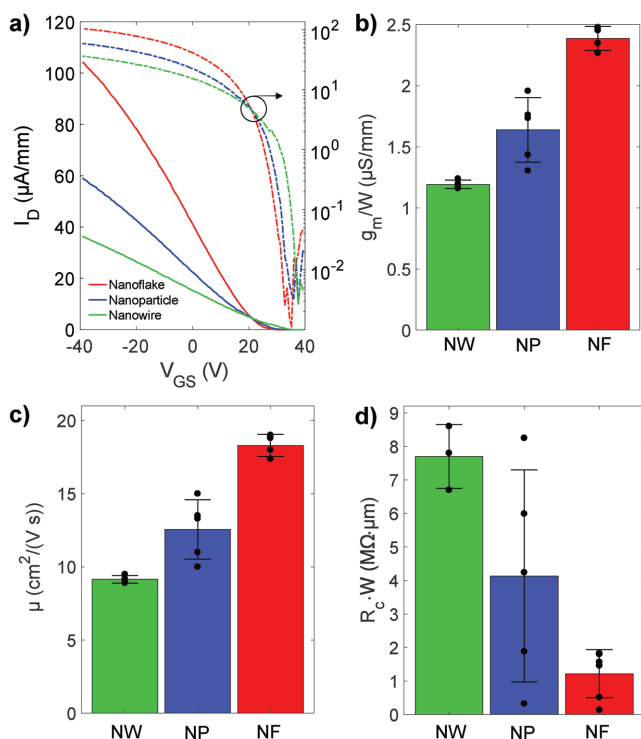


Figure 4. Electrical performance comparison between the silver contact morphologies in CNT-TFTs. a) Representative subthreshold and transfer characteristics between NF-contacted (red), NP-contacted (blue), and NW-contacted (green) devices. b) Transconductance and c) mobility comparison of Ag-contacted CNT-TFTs ($L_{ch} = 200$ μm), with each data point representing a single device. d) Contact resistance comparison using multiple TLM structures across different chips with each data point extracted from a distinct TLM structure. Error bars indicate the standard deviation.

Table 1. Benchmark comparison of solution processed or printed contact materials in CNT-TFTs. “—” indicates the metric was not reported in the original work.

Reference	Contact deposition process	Contact material	Contact geometry	L_{ch} [μm]	$g_{\text{m}}/w_{\text{ch}}$ [$\mu\text{S mm}^{-1}$]	μ [$\text{cm}^2 (\text{V}\cdot\text{s})^{-1}$]	$R_{\text{c}}\cdot w_{\text{ch}}$ [$\text{M}\Omega \mu\text{m}$]	Contact length [μm]	Max process temperature [$^{\circ}\text{C}$]
This work	Aerosol jet	Ag NF	Top	200	2.4	18.3	1.2	100–150	150
This work	Aerosol jet	Ag NP	Top	200	1.6	12.6	4.1	10–50	180
This work	Aerosol jet	Ag NW	Top	200	1.2	9.2	7.7	100–150	80
[20]	Aerosol jet	Ag NW	Top	180	1.4	11	8.3	120	80
[27]	Aerosol jet	m-CNT	Double	100	2.6	6.8	2.7	—	200
[27]	Aerosol jet	Au NP	Double	100	2.1	5.3	3.7	40	280
[27]	Aerosol jet	Ag NP	Double	100	1.3	3.2	6.5	30	200
[17]	Aerosol jet	Au NP	Bottom	50	2	11.5	—	10	300
[29]	Inkjet	Ag NP	Top	250	1.8	25	3.2	—	150
[22]	Inkjet	m-CNT	Top	150–200	0.11	4	—	450	150
[14]	Inkjet	Ag NP	Top	200	0.19	6.6	—	1100	200
[18]	Gravure	Ag NP	Top	85	2.5	4.3	—	170	150
[15]	Screen	Ag NP	Top	105	—	3.9	—	130	125
[24]	Screen	Ag NW	Bottom	50	—	33.8	—	175	150
[19]	Vacuum-filled microchannel	EGaIn	Top	200	0.98	3.42	45	230	150

from low-cost and highly conductive silver inks is not necessary to maximize CNT-TFT performance.

Based on our results, it may be hypothesized that solely increasing particle surface area will result in lower contact resistance; however, the relationships between particle size, aspect ratio, as well as surface area to volume ratio and their effects on the resulting process conditions and print quality all have to be taken into consideration. For this reason, although we found that silver NF contacts produce the highest performing CNT-TFTs, we ultimately conclude that contact morphology selection should be application specific. Due to the low resistivity and low contact resistance of silver NF films to CNT thin films, NF inks should be used whenever maximizing device and circuit performance is paramount. However, if higher printing resolution and density is required, silver NP films may be more favorable, depending on the ink characteristics and printing method. Notably, for very low-cost applications, printing NW inks with low-temperature process requirements can be advantageous due to their potential to circumvent the time and costs associated with high-temperature baking steps. Such low-temperature processing ability is also amenable for printing these conductive NW films onto temperature-sensitive materials. With technologies produced from printing methods expected to be tailorable for unique applications, these findings outline the trade-offs associated with contact morphology in CNT-TFTs, which is crucial for further development of low-cost printed electronic systems.

3. Conclusion

In summary, we have demonstrated that contact morphology plays a significant role in determining the overall on-state performance of CNT-TFTs. We investigated three different

silver contact morphologies, including NFs, NWs, and NPs, using two contact configurations (top- and bottom-contact). We found that NF top-contacts outperform all other contact materials and configurations, including those from reported works in the relevant literature. Additionally, we found that the top-contact configuration produces favorable uniformity characteristics, compared to bottom-contacts, for CNT-TFTs with channels that require solvent rinsing. In general, we conclude that contact morphology selection should be application specific, with NF contacts being selected for high performance, NP contacts for high resolution, and NW contacts for low-temperature process compatibility. The findings in this work address challenges associated with optimizing the use of silver inks in printed electronics for CNT-based devices, and in particular CNT-TFTs, which play a pivotal role in the formation of emerging technologies from low-cost printing methods.

4. Experimental Section

Substrate Preparation: Si/SiO₂ substrates were first ultrasonicated in acetone and isopropyl alcohol (IPA) for 5 min each, and then rinsed with deionized (DI) water and dried using an N₂ gun. The substrates were then subjected to an O₂ plasma (Emitech K-1050X) at 100 W for 4 min under low vacuum (0.6 Torr).

CNT Printing: Just prior to CNT printing, the SiO₂ surfaces were functionalized by immersion in PLL (0.1% w/v in water; Sigma-Aldrich) for 5 min followed by a thorough DI water rinse and dried using N₂. The channel region of every device produced in this work was fabricated using the following print parameters. High purity (>99%) single-walled semiconducting CNT ink (IsoSol-S100, Nanointegris Inc.) was diluted with toluene to a concentration of 0.01 mg mL^{−1} and then ultrasonicated to eliminate CNT aggregation that formed during the dilution process. Two milliliters of the resulting ink was then loaded into the ultrasonic atomizer of an Optomec AJ300 (Optomec Inc.) aerosol

jet printer and printed using a 150 μm nozzle, a sheath gas flow of 40 sccm, a carrier gas flow of 23 sccm, an ultrasonic transducer current of 330 mA, and a print speed of 1 mm s⁻¹ with two print passes to ensure sufficient CNT density.

Ag NF Printing: Fifteen to twenty milliliters of the Ag NF ink (HPS-108AE1, Novacentrix Inc.) was loaded into the pneumatic atomizer of the Optomec AJ300 and printed with the ink bath held at room temperature. The print parameters included a 300 μm nozzle diameter, a sheath gas flow rate of 45 sccm, an atomizer flow rate of 280 sccm, an exhaust flow rate of 260 sccm, and a print speed of 6 mm s⁻¹ with the platen temperature held at 60 °C. The resulting films were then baked in air at 150 °C for 1 h.

Ag NP Printing: To tune the viscosity of the Ag NP ink (Ag40x, UT Dots Inc.) for ultrasonic atomization, terpineol was added to the as-purchased solution in a 9:1 ratio by volume. Two milliliters of the resulting solution was then loaded into the ultrasonic atomizer of the Optomec AJ300. The print parameters included a 150 μm nozzle diameter, a sheath gas flow rate of 25 sccm, a carrier gas flow rate of 21 sccm, and an atomizer transducer current of 350 mA. The print speed was set to 3 mm s⁻¹ with and the platen temperature was held at 60 °C throughout printing. The resulting films were baked in air at 180 °C for 1 h.

Ag NW Ink and Printing: High aspect ratio Ag NWs were synthesized according to the polyol method as described in ref. [30]. The NWs were rinsed and then dispersed into IPA at a concentration of 4 mg mL⁻¹. High boiling point cosolvent ethylene glycol was then added (by 15% v/v) to the NW/IPA solution in order to improve film uniformity upon ink evaporation. Fifteen to twenty milliliters of the prepared ink was vortexed and then loaded into the pneumatic atomizer of the Optomec AJ300. With the ink bath kept at room temperature, Ag NWs were printed using a nozzle diameter of 300 μm , a sheath gas flow rate of 45 sccm, an atomizer gas flow rate of 280 sccm, and an exhaust flow rate of 260 sccm. The platen temperature was held at 80 °C throughout printing to assist with ink evaporation and film uniformity while the print speed was set to 3 mm s⁻¹ the platen temperature held at 60 °C throughout printing. The resulting films required no further post-processing. Further discussion on this ink and its printing can be found in previous work.^[20]

Characterization of Printed Materials and Devices: Optical images were taken using a Zeiss Axio Lab microscope with 2.5× to 100× objective lenses while a digital camera was used for image capture. SEM images of materials were acquired using a FEI XL30 (SEM-FEG). Electrical characterization was carried out in air using a table-top probe station along with a B1500A Device Analyzer (Keysight Technologies). Sheet resistance measurements were carried out using a 4-point probe method and a Keithley 2400 source measure unit. Profilometry measurements were carried out using a Zygo NewView 5000 (Zygo Corp.) optical profilometer.

Supporting Information

Supporting Information is available from the Wiley Online Library or from the author.

Acknowledgements

This work was supported by the Department of Defense Congressionally Directed Medical Research Program (CDMRP) under award number W81XWH-17-2-0045. J.A.C. acknowledges support from the National Science Foundation (NSF) through the NSF graduate research fellowship (grant no. DGE11010101-0417-7172-7172/4103). This work was performed in part at the Duke University Shared Materials Instrumentation Facility (SMIF), a member of the North Carolina Research Triangle Nanotechnology Network (RTNN), which was supported by the National Science Foundation (Grant ECCS-1542015) as part of the National Nanotechnology Coordinated Infrastructure (NNCI).

Conflict of Interest

The authors declare no conflict of interest.

Keywords

carbon nanotube (CNT), contact resistance, printed silver, thin-film transistor (TFT)

Received: August 16, 2018

Revised: October 19, 2018

Published online: November 13, 2018

- [1] Y. Zhan, Y. Mei, L. Zheng, *J. Mater. Chem. C* **2014**, 2, 1220.
- [2] Z. Bao, X. Chen, *Adv. Mater.* **2016**, 28, 4177.
- [3] A. Nathan, A. Ahnood, M. T. Cole, S. Lee, Y. Suzuki, P. Hiralal, F. Bonaccorso, T. Hasan, L. Garcia-Gancedo, A. Dyadyusha, S. Haque, *Proc. IEEE* **2012**, 100, 1486.
- [4] G. Yang, L. Xie, M. Mäntysalo, X. Zhou, Z. Pang, L. Da Xu, S. Kao-Walter, Q. Chen, L. R. Zheng, *IEEE Trans. Ind. Inf.* **2014**, 10, 2180.
- [5] G. Hu, J. Kang, L. W. Ng, X. Zhu, R. C. Howe, C. G. Jones, M. C. Hersam, T. Hasan, *Chem. Soc. Rev.* **2018**, 47, 3265.
- [6] A. D. Franklin, *Science* **2015**, 349, aab2750.
- [7] K. Rajan, I. Roppolo, A. Chiappone, S. Bocchini, D. Perrone, A. Chiolerio, *Nanotechnol., Sci. Appl.* **2016**, 9, 1.
- [8] J. Perelaer, P. J. Smith, D. Mager, D. Soltman, S. K. Volkman, V. Subramanian, J. G. Korvink, U. S. Schubert, *J. Mater. Chem.* **2010**, 20, 8446.
- [9] S. B. Walker, J. A. Lewis, *J. Am. Chem. Soc.* **2012**, 134, 1419.
- [10] J. M. Yun, J. S. Yeo, J. Kim, H. G. Jeong, D. Y. Kim, Y. J. Noh, S. S. Kim, B. C. Ku, S. I. Na, *Adv. Mater.* **2011**, 23, 4923.
- [11] L. Xiang, H. Zhang, G. Dong, D. Zhong, J. Han, X. Liang, Z. Zhang, L. M. Peng, Y. Hu, *Nat. Electron.* **2018**, 1, 237.
- [12] J. B. Andrews, J. A. Cardenas, C. J. Lim, S. G. Noyce, J. Mullett, A. D. Franklin, *IEEE Sens. J.* **2018**, 18, 7875.
- [13] J. Tang, Q. Cao, G. Tulevski, K. A. Jenkins, L. Nela, D. B. Farmer, S. J. Han, *Nat. Electron.* **2018**, 1, 191.
- [14] D. Lee, J. Yoon, J. Lee, B. H. Lee, M. L. Seol, H. Bae, S. B. Jeon, H. Seong, S. G. Im, S. J. Choi, Y. K. Choi, *Sci. Rep.* **2016**, 6, 26121.
- [15] X. Cao, C. Lau, Y. Liu, F. Wu, H. Gui, Q. Liu, Y. Ma, H. Wan, M. R. Amer, C. Zhou, *ACS Nano* **2016**, 10, 9816.
- [16] C. Cao, J. B. Andrews, A. D. Franklin, *Adv. Electron. Mater.* **2017**, 3, 1700057.
- [17] H. Li, Y. Tang, W. Guo, H. Liu, L. Zhou, N. Smolinski, *Adv. Funct. Mater.* **2016**, 26, 6914.
- [18] P. H. Lau, K. Takei, C. Wang, Y. Ju, J. Kim, Z. Yu, T. Takahashi, G. Cho, A. Javey, *Nano Lett.* **2013**, 13, 3864.
- [19] J. B. Andrews, K. Mondal, T. Neumann, J. A. Cardenas, J. Wang, D. P. Parekh, Y. Lin, P. Ballentine, M. D. Dickey, A. D. Franklin, *ACS Nano* **2018**, 12, 5482.
- [20] J. A. Cardenas, M. J. Catenacci, J. B. Andrews, N. X. Williams, B. J. Wiley, A. D. Franklin, *ACS Appl. Nano Mater.* **2018**, 1, 1863.
- [21] J. Liang, L. Li, D. Chen, T. Hajagos, Z. Ren, S. Y. Chou, W. Hu, Q. Pei, *Nat. Commun.* **2015**, 6, 7647.
- [22] L. Cai, S. Zhang, J. Miao, Z. Yu, C. Wang, *ACS Nano* **2016**, 10, 11459.
- [23] C. Zhu, A. Chortos, Y. Wang, R. Pfattner, T. Lei, A. C. Hinckley, I. Pochorovski, X. Yan, J. W. F. To, J. Y. Oh, J. B. H. Tok, *Nat. Electron.* **2018**, 1, 183.

- [24] J. Liang, K. Tong, Q. Pei, *Adv. Mater.* **2016**, 28, 5986.
- [25] F. Xu, M. Y. Wu, N. S. Safron, S. S. Roy, R. M. Jacobberger, D. J. Bindl, J. H. Seo, T. H. Chang, Z. Ma, M. S. Arnold, *Nano Lett.* **2014**, 14, 682.
- [26] K. Chen, W. Gao, S. Emaminejad, D. Kiriya, H. Ota, H. Y. Y. Nyein, K. Takei, A. Javey, *Adv. Mater.* **2016**, 28, 4397.
- [27] C. Cao, J. B. Andrews, A. Kumar, A. D. Franklin, *ACS Nano* **2016**, 10, 5221.
- [28] J. Yoon, M. Lim, B. Choi, D. M. Kim, D. H. Kim, S. Kim, S. J. Choi, *Sci. Rep.* **2017**, 7, 5453.
- [29] Y. Lee, J. Yoon, B. Choi, H. Lee, J. Park, M. Jeon, J. Han, J. Lee, Y. Kim, D. H. Kim, D. M. Kim, *Appl. Phys. Lett.* **2017**, 111, 173108.
- [30] I. E. Stewart, M. J. Kim, B. J. Wiley, *ACS Appl. Mater. Interfaces* **2017**, 9, 1870.
- [31] D. K. Schroder, *Semiconductor Material and Device Characterization*, John Wiley & Sons, Hoboken, New Jersey **2006**.